Hybrid Modulation of Dual Inverter for Open-End Permanent Magnet Synchronous Motor

Yongjae Lee, *Student Member, IEEE*, and Jung-Ik Ha, *Senior Member, IEEE*

***Abstract*—This paper analyzes the dual inverter driven open-end permanent magnet synchronous motor (PMSM) system and proposes control method which can generate maximum output power in overall speed range for integrated starter/alternator. Dual inverter driven open-end machine system consists of two inverters which are connected to the both ends of the machine winding. By disconnecting one inverter from the power source, the dc-link voltage of flying capacitor can be boosted through the machine. Because one inverter is connected to the only power source, output power of the machine is regulated by the source connected inverter. In this paper, modulation method for maximizing output power of inverter and motor with reduced harmonic and loss is proposed. It is a hybrid modulation combining six-step and pulse width modulations. With proposed method, efficiency and operation area are improved and cost of entire driving system is also decreased due to the removing of dc–dc converter. Analyses, strategies, control method, and simulation results are descripted. The experiments with PMSM are accomplished to verify the feasibility of proposed method.**

***Index Terms*—Dual inverter, harmonic reduction, integrated starter/alternator (ISA), open-end winding, permanent magnet synchronous motor (PMSM) drive.**

I. Introduction

RECENTLY, because of the environmental problem and soaring of the fuel price, electric motor systems are adopted to the many kinds of traction applications such as train and vehicle which were traditionally driven by internal combustion engine (ICE) or external combustion engine (ECE). In addition, because efficiency of the electric traction system is higher than that of ICE, electric traction vehicles have higher mileage than the ICE vehicles. It is expected that efficiency of the future hybrid electric vehicle (HEV) and electric vehicle (EV) becomes higher than the current level thanks to the improvements of the inverter topology, switching devices, and motor design technologies.

AC motors, permanent magnet synchronous motors (PMSMs), and induction motors, are generally used as a traction motor for HEV due to their high efficiency although complex control technique is required. Among the ac motors, PMSMs are mostly used in HEV because of their high efficiency and compactness. Especially, interior permanent magnet synchronous motor (IPMSM) is suitable for HEV application due to its reluctance torques in field weakening region. Because the required operating region of HEV motor is much wider than that of other applications, the reluctance torque and wide field weakening characteristic make IPMSM adopted for traction motor of EV.

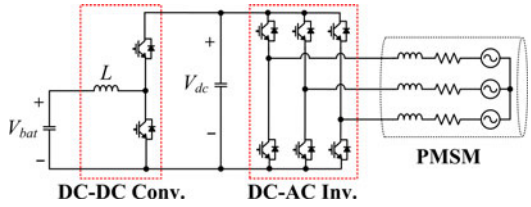

Fig. 1. PMSM drive with dc–dc converter.

The high efficiency of PMSM mainly comes from its inherent rotor flux from permanent magnet, whereas other motors need the rotor current for generating the rotor flux. Thanks to this rotor flux, efficiency below the rated speed is higher than other motors and the power factor of the PMSM is also higher than that of other machines. However, this constant rotor flux generates high back-electromotive force (back-EMF) in the high speed region. Because output voltage of the inverter should be controlled under the available range, field weakening control is necessary for the high speed operation [1]–[8]. The negative *d*-axis current reduces back-EMF and lowers the required voltage. Thus, system can be maintained in the stable operation. Although IPMSM shows higher efficiency than that of other PMSMs in high speed region, it is true that field weakening current restricts output torque and drops the efficiency. By these reasons, high dc-link voltage is required to reduce the field weakening current and secure the high speed operation of HEV. However, it is hard to make high dc-link voltage directly from the battery because stacking of battery cells requires complex cell balancing circuits [9]–[13]. Most of all, high battery voltage is potentially dangerous. So, dc–dc boost converter is generally used to make high dc-link voltage from relatively low battery voltage. The simple schematic of drive system with such dc–dc converter is shown in Fig. 1. This kind of cascaded system, however, deteriorates the system efficiency. The boosting ratio of dc–dc converter is also not high, normally between 2 and 3, because high boosting ratio lowers efficiency. Because inductor used in dc–dc converter takes huge volume and weight, it is also pointed out as a drawback of dc–dc converter [14], [15].

To overcome the demerits of the cascaded system with the dc–dc converter, several studies have been conducted. Z-source inverter proposed by Peng *et al.* is one of those studies [16]–[19]. Z-source inverter uses no dc–dc converter and makes circuit

Manuscript received March 31, 2014; accepted May 5, 2014. Date of publication May 19, 2014; date of current version January 16, 2015. This work was supported by the National Research Foundation of Korea under Grant 2009-0083495 funded by the Ministry of Science, ICT & Future Planning. Recommended for publication by Associate Editor B. Lehman.

The authors are with the Department of Electrical and Computer Engineering, Seoul National University, Seoul, Korea (e-mail: yongjaelee@snu.ac.kr; jungikha@snu.ac.kr).

Color versions of one or more of the figures in this paper are available online at http://ieeexplore.ieee.org

Digital Object Identifier 10.1109/TPEL.2014.2325738

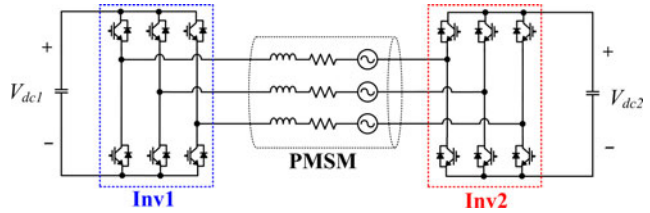

Fig. 2. PMSM drive with dual inverter with flying inverter.

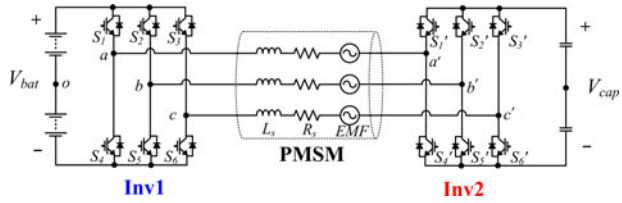

Fig. 3. Electrical schematic of dual inverter with flying inverter.

simpler with inductors and capacitors. It also has a strong fault tolerance because it removes dead time between upper and lower switch. However, it is far from reducing the volume and weight because it requires two inductors and capacitors. The boosting ratio is also restricted by output voltage and shoot-through zero state. In [15], the cascaded H-bridge with flying capacitor is proposed to obtain higher output voltage. This method, however, requires not only many switches but also the complicated look-up table. The modulation index (MI) is also limited by the load condition.

Dual inverter also can be used to obtain high phase voltage for HEV without dc–dc converter because each phase can be considered as full-bridge converter. The previous researches about the dual inverter topology can be classified into three groups according to the topics; multilevel inverter [20]–[26], system integrator [27]–[30], and boost function [31]–[35]. This paper especially focused on the boosting capability of dual inverter system. In [31], dual inverter with flying capacitor shown in Fig. 2 was proposed. They used the isolated flying inverter as reactive power source. They proposed the decoupling control method and flying dc-link voltage regulation method for the dual inverter with flying capacitor. In [32], dual inverter with flying capacitor is modeled as series connected inductor. However, there are several problems such as costs, size, and relatively low efficiency due to the high inverter loss. In order to improve the efficiency, Ewanchuk *et al.* studied about the operation of the dual inverter with flying capacitor when six-step operation is adopted for both inverters [33]. In [34], common mode power transferring method by dual inverter system is examined. Jayasinghe *et al.* proposed wind energy conversion system with dual inverter concept [28], [29]. They used efficient IGCTs for the generator side inverter for the six-step modulation method. They also presents the compensation modulation method to make sinusoidal output current. However, the further consideration and control methods are required when it comes to the motor driving applications.

This paper presents the control strategy for dual inverter fed open-end motor with flying capacitor as shown in Fig. 2. The proposed hybrid modulation method consists of the six step of the input side inverter, *Inv*1, and pulse width modulation (PWM) of the isolated inverter, *Inv*2. By applying the proposed hybrid modulation method, the operation area is expanded in high-speed region. The efficiency is increased and the size can be also reduced because the losses by the power device switching and the field weakening current are reduced. The control objects of the proposed dual inverter with flying capacitor system include not only the output torque but also the flying capacitor voltage. For this control, the power flows between two inverters and the motor are considered simultaneously. While the six step generates the ripple power, the method proposed in this paper eliminates the ripples using PWM of the isolated inverter. This paper presents the details of the previous research [35] which had shown the feasibility of the hybrid modulation method and proposes phase shift hybrid modulation method.

This paper organized as follows. In Section II, electrical model of the PMSM is introduced and the power flow of the dual inverter scheme is analyzed. In Section III, hybrid modulation method for dual inverter system is proposed and the expanded operation area is analyzed. In Section IV, experimental results with open-end PMSM are presented. And conclusion of this paper is given in Section V.

II. Basics of Operation

The dual inverter system with flying capacitor satisfies the two main objects: load power regulation and flying dc-link voltage regulation. The former is for following the user command and the latter is for safe operation of the isolated inverter with flying capacitor. This section describes the control method satisfying the objects in the dual inverter with flying capacitor topology. Such an objective can be accomplished with voltage decoupling control proposed in [31]. The constraints of the proposed system and the advantages of dual inverter topology with flying capacitor are described in this section.

A. System Modeling

In analyzing the modulation method and power flow, the electrical model of PMSM and dual inverter is considered. Fig. 3 shows the electrical schematic of dual inverter and PMSM. PMSM is simply modeled with inductor, resistor, and back-EMF from electromagnetic coupling. The open stator windings are connected to the legs of *Inv*1 and *Inv*2.

*Inv*1 connected to the battery is drawn at the left side of Fig. 3 and *Inv*2 connected to the capacitor bank is at the opposite end. Terminals and switches of the *Inv*2 are expressed with prime for easy contrast.

Pole voltages of *Inv*1 are V_{ao}, V_{bo}, and V_{co}, and pole voltages of *Inv*2 are $V_{a'o'}$, $V_{b'o'}$, and $V_{c'o'}$. Phase voltages applied to the motor are expressed as

$$\begin{aligned} V_{aa'} &= V_{ao} - V_{a'o'} + V_{oo'} \\ V_{bb'} &= V_{bo} - V_{b'o'} + V_{oo'} \\ V_{cc'} &= V_{co} - V_{c'o'} + V_{oo'} \end{aligned} \tag{1}$$

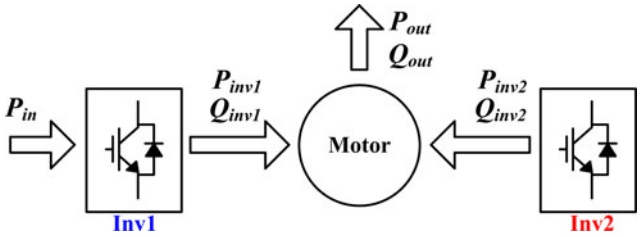

Fig. 4. Power flow diagram of dual inverter system.

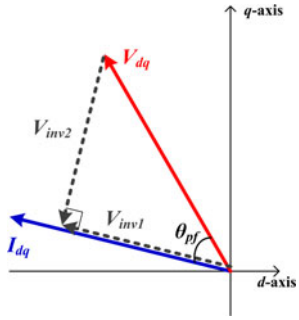

Fig. 5. Vector diagram of current and decoupled voltage.

where the common mode voltage between both inverters, V_{oo}', is defined as

$$V_{oo'} = (V_{ao} + V_{bo} + V_{co})/3 - (V_{a'o'} + V_{b'o'} + V_{c'o'})/3. \quad (2)$$

This common mode voltage does not contribute to the torque generation because only differential components generate torque. In the rotating reference frame, voltage to the motor can also be written as

$$\begin{aligned} V_d &= V_{d,inv1} - V_{d,inv2} \\ V_q &= V_{q,inv1} - V_{q,inv2} \end{aligned} \quad (3)$$

where V_d and V_q are the *d–q* stator voltages in the synchronous reference frame rotating at the angular velocity ω_r. $V_{d,inv1}$ and $V_{q,inv1}$ are the *d–q* output voltages of *Inv*1 and $V_{d,inv2}$ and $V_{q,inv2}$ are the *d–q* output voltages of *Inv*2 in the synchronous reference frame, respectively.

The voltage and torque equations for PMSM in the synchronous reference frame are written as

$$V_d = R_s I_d + pL_d I_d - \omega_r L_q I_q \quad (4)$$

$$V_q = R_s I_q + pL_q I_q + \omega_r(\lambda_f + L_d I_d) \quad (5)$$

$$T_e = \frac{3}{2}\frac{n_p}{2}[\lambda_f + (L_d - L_q)I_d]I_q \quad (6)$$

where I_d and I_q are the *d–q* stator currents in the synchronous reference frame. Resistance and inductances of the stator are denoted as R_s, L_d, and L_q. p indicates differential operator (d/dt), λ_f is rotor flux, and n_p is number of the poles.

B. Power Control

Fig. 4 demonstrates the power flow diagram of dual inverter with flying capacitor system. *P* and *Q* indicate the active and reactive powers, respectively. The subscripts indicate the power source. P_{in} shows the input power to the system and P_{out} and Q_{out} show the active and reactive powers consumed by the machine.

As aforementioned, main objects of the machine drive system by dual inverter with flying capacitor system are torque or speed regulation of the machine and flying dc-link voltage regulation. To accomplish the first object, P_{out} and Q_{out} are regulated. And the active power flow of the *Inv*2, P_{inv2}, is controlled to zero in order to accomplish the second object. Reactive power is irrelevant to the flying dc-link voltage because input and output active powers only change dc-link voltage. This is common idea for the isolated power systems as in the static synchronous compensator (STATCOM) [36]. It can be summarized as

$$P_{inv2} = 0. \quad (7)$$

Because P_{out} and Q_{out} are regulated by motor controller, the following equations can be induced from (7) in ideal lossless system

$$P_{in} = P_{inv1} = P_{\text{out}} \quad (8)$$

$$Q_{inv1} + Q_{inv2} = Q_{\text{out}}. \quad (9)$$

Currents flowing in the system are identical in inverters and motor. Thus, output powers of the each component are varied with output voltages of inverters. P_{inv2} becomes zero when the amplitude of output voltage of the *Inv2*, V_{inv2}, is zero or the angle difference between current and V_{inv2} is 90°. At the same time, reactive power of the *Inv*1, Q_{inv1}, should be controlled to zero to maximize the output active power because the apparent output power is limited by dc-link voltage connected to the power source when the constant current flows. Therefore, the reactive powers are controlled as

$$\begin{aligned} Q_{inv1} &= 0 \\ Q_{inv2} &= Q_{\text{out}}. \end{aligned} \quad (10)$$

Equation (10) indicates that the reactive power required to the motor is supplied by flying inverter. In other words, flying inverter works as a reactive power source.

C. Powers and Voltages

In the conventional control method, output voltages of the components are determined to satisfy the aforementioned conditions [31], [32]. The previous researches give the ideas of making two output voltages orthogonal to maximize the output power while decoupling the power. Fig. 5 shows the vector diagram of the conventional control method. By putting the output voltage Vector of the V_{inv1} in parallel with the current vector, it is possible to maximize the P_{inv1}. Simultaneously, V_{inv2} is decided to orthogonal to the current vector to eliminate the active power flow to *Inv2*. Thus, (7), (8), and (10) are satisfied regardless of the operation condition.

In the case of the general machine drive system using only one inverter, the required power from the machine is entirely

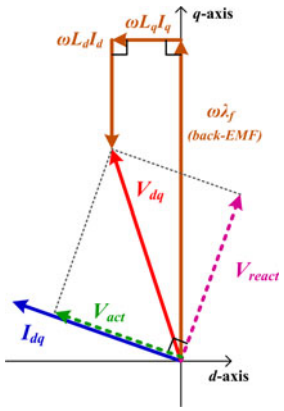

Fig. 6. Vector diagram of IPMSM in high speed region.

supplied by the single inverter. For the dual inverter with flying capacitor system, however, source connected inverter only takes charge of not the apparent power but the real power. Thus, constant active power can be supplied irrespective of load condition, while flying capacitor supplies reactive power. In summary, active output power in the low power factor region can be increased in the dual inverter system with flying capacitor.

General PMSM shows relatively high power factor at low speed and around the rated speed. Thus, the required reactive power is also not high. For the high speed region, however, negative *d*-axis current is definitely necessary to reduce the back-EMF induced by the rotor permanent magnets. Fig. 6 shows the current and voltage vectors of IPMSM in high speed region. Because the resistive voltage drop is much smaller than the voltage from magnetic coupling, the resistive voltage is neglected in the vector diagram of Fig. 6. The small dynamic voltage terms are also neglected in the diagram. As shown in Fig. 6, the angle difference between current and voltage vectors is considerable in the high speed region. Thus, the reactive voltage, V_{react}, is also high as much as the active voltage, V_{act}. The faster the machine rotates, the higher reactive voltage is required. Existence of the flying inverter and capacitor lightens the burden of reactive power and helps the efficient high speed drive.

III. Hybrid Modulation of Dual Inverter With Flying Capacitor

In this section, power enhancement method using six-step modulation is proposed. Principle of operation is explained by comparing the proposed method with the conventional methods. This section also includes the analyses of proposed six-step modulation of dual inverter with flying capacitor scheme focusing on the power and voltage. To widen the operation of hybrid modulation method, phase shifting of six-step modulation method is also proposed. Field weakening control method which is essential for the high speed operation for the proposed modulation method is also suggested in this section.

TABLE I
Modulation Indices

Modulation method	MI	Amplitude of first harmonic
SPWM	0.7854	$0.5\ V_{\mathrm{dc}}$
SVPWM	0.9067	$1/\sqrt{3}\ V_{dc}$
Six Step	1.0	$2/\sqrt{\pi}\ V_{dc}$

A. Principle and Objectives

Six-step modulation is widely known as a modulation method which can generate maximum output voltage. Table I shows the maximum output voltage of the three representative modulation methods; sinusoidal PWM (SPWM), space vector PWM (SVPWM), and six-step modulation. Six-step modulation shows approximately 10% higher output voltage than SVPWM method. In addition, the switching loss also reduced, because only one switching is required in a period. Although the six-step modulation maximizes the amplitude of fundamental frequency component, it generates odd harmonics which lower the efficiency and cause the torque ripple and noise. It is also hard to apply to the machine which has small inductance because of the instant current soaring. Thus, it is temporarily used in dynamic situation such as rapid acceleration or the applications where the above defects are acceptable.

For the dual inverter topology, the voltage applied to the load is decided as a difference of the voltages from two inverters. Thus, the output voltage of the one inverter does not directly affect the load. This characteristic enables the hybrid modulation of dual inverter topology. In the proposed hybrid modulation method, input side inverter modulates the output voltage with six-step. At the same time, opposite inverter compensates the odd harmonics generated from input side inverter. Thanks to the compensation of the flying inverter, load voltage, and current are maintained in sinusoidal form without harmonics. In summary, proposed method takes advantages of the six-step modulation such as low switching loss and high output power and removes the disadvantages such as high order harmonics and torque ripple.

The hybrid modulation suggested in [28] and [29] uses the same characteristics of the dual inverter topology. However, the huge battery bank is hard to apply to the flying dc-link capacitor in the motor drive application. Furthermore, the battery bank also can be recognized as isolated power source not a small dc-link capacitor. Because the six-step modulation generates fluctuating active power, voltage of the small dc-link capacitor also fluctuates. Thus, the ripple power from the six-step operation need to be analyzed and it is accomplished in the following section.

B. In-Phase Six-Step Operation

As briefly mentioned, the proposed in-phase six-step modulation for dual inverter topology with flying capacitor features the six-step of an input side inverter and the harmonic compensation of a flying inverter. It maximizes the output power

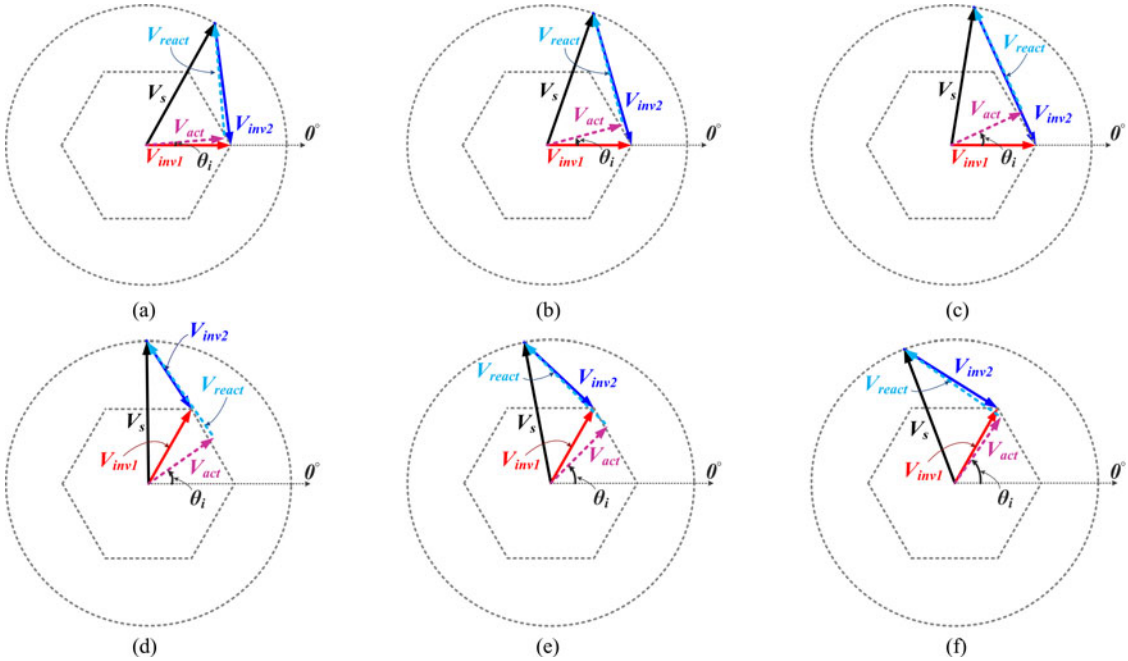

Fig. 7. Vector diagrams of proposed six step modulation in stationary reference frame according to the angle of current. (a) 5°, (b) 15°, (c) 25°, (d) 35°, (e) 45°, (f) 55°.

of the machine and increases the power density of the drive system. The opposite case where the six step of the flying inverter and the harmonic compensation of the input side inverter is also feasible, but the output power is reduced because the active voltage output of the input side inverter is reduced. Applying the six-step to both inverters is also possible but it generates lots of current harmonics and torque ripples [33]. In addition, because the output voltage of the six-step modulation is decided by the dc-link voltage, both of the dc-link voltages should be controlled to supply the voltage required by the load.

Vector diagrams of the in-phase six-step modulation method are shown in the Fig. 7. It represents how the vectors rotate in the stationary reference frame. The voltage reference vector, V_s, is divided into $V_{\rm act}$ and $V_{\rm react}$ with the broken arrow. V_s is also represented as the subtraction of two output voltage vectors, V_{inv1} and V_{inv2}, with solid arrows. Because the output voltage is the subtraction of the two vectors, the arrow of the V_{inv2} heads the same point with that of the V_{inv1}. The direction of the current vector is same with that of $V_{\rm act}$. As the current vector rotates counterclockwise from (a) to (c), V_s, $V_{\rm act}$, and $V_{\rm react}$ rotate together. The voltage references of each inverter, however, are decided to point the vertex which is located at the right side of the voltage hexagon of the input side inverter, vertex no. 1 in Table II, because this vertex is the point where the active output voltage of the *Inv1* is maximized. When the current vector rotates over 30° as in Fig. 7(d), V_{inv1} and V_{inv2} point the next vertex in counterclockwise direction, vertex no. 2 in Table II. As same with the cases of Fig 7(a), (b), and (c), V_{inv1} and V_{inv2} in Fig 7(d), (e), and (f) do not move from the vertex located at 60°. In summary, V_{inv1} is decided by the angle of the current as depicted in Table II and V_{inv2} is decided as (11)

$$V_{inv2} = V_{inv1} - V_s. \tag{11}$$

For example, if the current vector is laid on 120°, V_{inv1} points the vertex no. 3 in Table II.

Fig. 8 shows the decomposed vector diagram of six-step modulated V_{inv1} when current vector located in 80°. V_{inv1} is decided on the vertex no. 2 and can be divided into active component $V_{inv1,\rm act}$ and reactive component $V_{inv1,\rm react}$. $V_{inv1,\rm act}$ can be achieved by projecting the V_{inv1} to the current vector. As shown in the Fig. 8, $V_{inv1,\rm act}$ is always located outside of the voltage hexagon. By projecting the six step modulated V_{inv1} for every current angle, trajectory of the $V_{inv1,\rm act}$ can be drawn as depicted in Fig. 8. It shows that the length of the $V_{inv1,\rm act}$ is not constant and varies according to the current angle. Thus, output power is fluctuating even in the steady state.

TABLE II
SIX-STEP VECTOR

Current angle	Vertex number	Switching states					
		S_1	S_2	S_3	S_4	S_5	S_6
$-30° \le \theta_{\rm i} < 30°$	1	on	off	off	off	on	on
$30° \le \theta_{\rm i} < 90°$	2	on	on	off	off	off	on
$90° \le \theta_{\rm i} < 150°$	3	off	on	off	on	off	on
$150° \le \theta_{\rm i} < 180°$, $-180° \le \theta_{\rm i} < -150°$	4	off	on	on	on	off	off
$-150° \le \theta_{\rm i} < -90°$	5	off	off	on	on	on	off
$-90° \le \theta_{\rm i} < -30°$	6	on	off	on	off	on	off

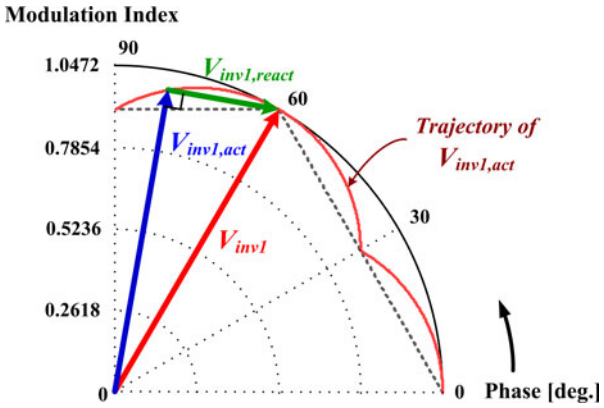

Fig. 8. Vector disassembling analysis of six step modulation method in the stationary reference frame from 0° to 90°.

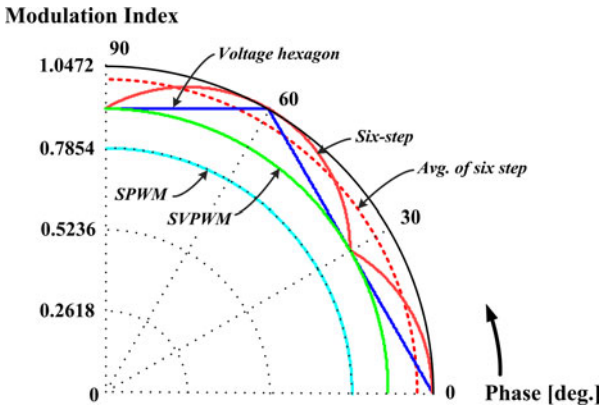

Fig. 9. Comparison of active voltage output according to the modulation methods in the stationary reference frame from 0° to 90°.

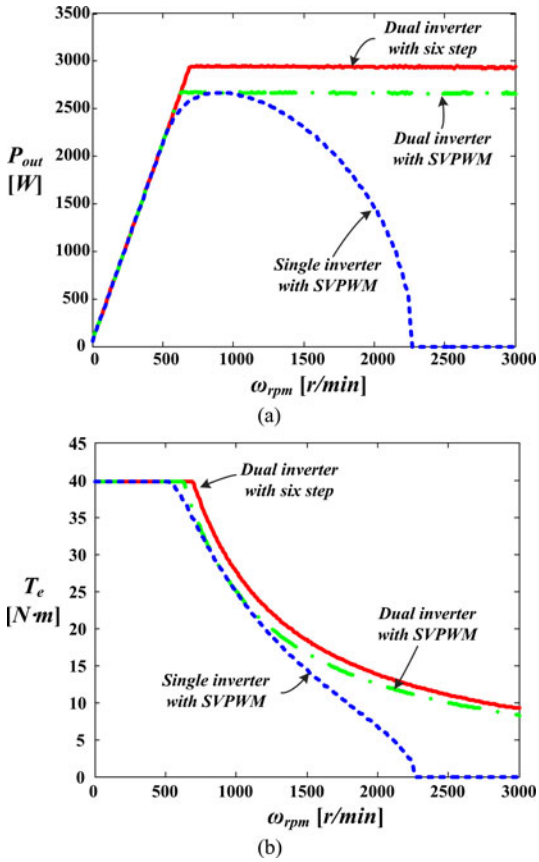

Fig. 10. Torque/speed and power/speed curves of the SPMSM with single inverter with SVPWM, dual inverter with SVPWM, and dual inverter with six step. (a) Torque/speed curve. (b) Power/speed curve.

Fig. 9 shows the active output voltages of the various PWM methods for easy comparison. For the conventional PWM methods such as SVPWM and SPWM, maximum linear output voltage of the inverter can be drawn as circle with constant radius. However, instantaneous active voltage output of the six-step modulation is not constant. The average of the active voltage in the six-step modulation is much higher than other linear PWM methods. Thus, the higher power can be transferred between the power source and the machine.

The increased output power enhances output torque in the high speed region. Because the output voltage of the *Inv*1 is increased, field weakening current for reducing the active voltage is reduced in comparison to the other PWM methods. In other words, higher currents can be used to generate torque instead of reducing the flux. Fig. 10 shows the torque/speed and output power/speed curves of the single inverter system, dual inverter system using SVPWM, and dual inverter system using six-step. In the low speed region, torque output of the three methods are identical because required voltage is located inside of the linear region. Thus, output torque is only limited by the current rating. In the high speed region, however, the voltage required by the machine goes higher and cannot be supplied by the inverter. For the single inverter case, the *d*-axis current is injected to reduce the output voltage till the voltage goes inside the synthesizable voltage range. Thus, output torque is reduced rapidly above the rated speed. For the dual inverter case, on the other hand, the active voltage is only limited because flying inverter supplies reactive voltage. Thus, output torque is maintained over the rated speed of the single inverter case. When the required active voltage reaches the maximum output voltage of the *Inv*1, *d*-axis current is injected to reduce the required active voltage. If the dc-link voltage of the *Inv*2 can be boosted enough, output power of the dual inverter system is maintained as shown in Fig. 10(b). Because the active power is constant, output torque of the dual inverter system is reduced in inverse proportion to the rotating speed of the machine as illustrated in Fig. 10(a). In the constant power region, output torque and power of the machine are decided by voltage rating of the *Inv*1. Thus, output power and torque in the proposed six-step modulation are higher than those in the conventional method.

Furthermore, the six-step modulation of dual inverter system provides continuous battery current. Linear PWM methods chop the phase current with the switching and make dc-link current discontinuous [37]. This harmonic current to the battery should be reduced because it shortens the lifetime of the battery [38]. In the systems of which the battery is directly connected to

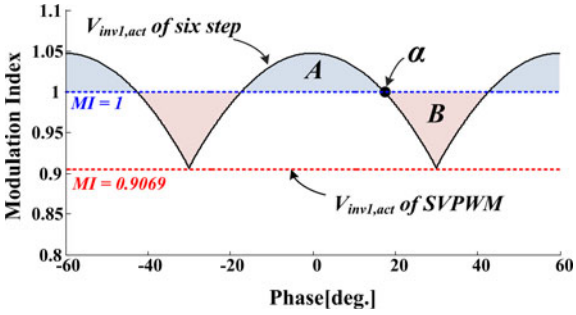

Fig. 11. Active output voltage of the six step modulated voltage in Cartesian coordinate from −60° to 60°.

the battery, especially, the negative effect is much severer because the dc-link harmonic current directly affects the battery. To solve this problem, the system requires a huge electrolytic capacitor to reduce the switching current. Because the proposed six-step method provides continuous dc-link current which is not chopped by switching, filter capacitor can be reduced. Although dc-link current of the proposed method contains the harmonics from *Inv*2, it is much smaller than the chopped current because the current is filtered by machine inductance.

Although six-step modulation maximizes the active output power, the reactive voltage $V_{inv1,\mathrm{react}}$ is additionally generated because the phase difference exists between output voltage and current vector as shown in the Fig. 8. The reactive voltage generated from *Inv*1 is maximized when the angle difference between current vector and output voltage is maximized. Because the maximum angle difference is 30°, maximum value of the additional reactive voltage from the in-phase six step modulated *Inv*1 can be depicted as

$$\max|V_{inv1,\mathrm{react}}| = \frac{2}{3}V_{\mathrm{dc1}} \times \cos 30^\circ = \frac{1}{\sqrt{3}}V_{\mathrm{dc1}}. \tag{12}$$

This additional reactive voltage should be compensated by *Inv*2 to regulate the machine current. Thus, dc-link voltage of the *Inv*2, V_{dc2}, should be controlled to handle the reactive voltage from the *Inv*1. Due to this additional dc-link voltage, the switching loss of the *Inv*2 is slightly higher than that of the SVPWM is used. Though the compensation of fluctuating active voltage also requires increment of dc-link voltage, the effect of fluctuating active voltage of *Inv*1 to increment of V_{dc2} is negligible.

Because the P_{inv1} fluctuates according to the V_{inv1}, P_{inv2} should be fluctuated to maintain P_{out} constant. As mentioned in the previous section, it is obvious that nonzero P_{inv2} varies V_{dc2}. Although the average of P_{inv2} is controlled to zero, fluctuating power from the six step fluctuates V_{dc2}. Fig. 11 shows the amplitude of six-step modulated voltage vector according to the phase angle from −60° to 60°. The active voltage of the six step modulated *Inv*1 is represented as blue solid line and its average value is 1 MI. Fluctuating dc-link voltage is determined with the integrated power to the capacitor and indicated by A and B in Fig. 11. Though Fig. 11 represents the voltage magnitude, it is proportional to the power when the currents flowing in the load are sinusoidal. Because the areas of A and B are same and the curve is even function, the area is easily calculated by integrating from 0° to α. α represents the crossing point of the average voltage and instant voltage which is calculated as

$$\frac{2}{3}V_{\mathrm{dc1}}\cos\theta_\alpha = \frac{2}{\pi}V_{\mathrm{dc1}}. \tag{13}$$

Then, θ_α is calculated as

$$\theta_\alpha = \cos^{-1}\left(\frac{\frac{2}{\pi}V_{\mathrm{dc1}}}{\frac{2}{3}V_{\mathrm{dc1}}}\right) = \cos^{-1}\left(\frac{3}{\pi}\right) = 16.267^\circ. \tag{14}$$

Thus, energy transferred in area *A*, E_A, can be calculated with

$$E_A = 2\cdot 1.5\cdot I_s\cdot V_{\mathrm{dc1}}\frac{1}{2\pi f}\int_0^{\theta_\alpha}\left(\frac{2}{3}\cos\theta - \frac{2}{\pi}\right)\mathrm{d}\theta \tag{15}$$

where I_s is amplitude of phase current and *f* is the fundamental frequency of current. V_{dc2} is maximized at the right edge of *A* and minimized at the right edge of *B*. The relationship between fluctuating energy and voltage can be descripted as

$$\begin{aligned} E_A &= \frac{1}{2}C_2\left(V_{\max}^2 - V_{\min}^2\right) \\ &= \frac{1}{2}C_2\left((V_{\mathrm{avg}}+\Delta V)^2 - (V_{\mathrm{avg}}-\Delta V)^2\right) \\ &= 2C_2V_{\mathrm{avg}}\Delta V \end{aligned} \tag{16}$$

where C_2 is the capacitance of the flying dc-link capacitor, $V_{\max}$ and $V_{\min}$ are maximum and minimum values of the V_{dc2}, respectively, V_{avg} is the average value of V_{dc2}, and ΔV is the amplitude of the fluctuating voltage. From (15) and (16), amplitude of fluctuating voltage is depicted as

$$\Delta V = k(0)\frac{V_{\mathrm{dc1}}I_s}{fC_2V_{\mathrm{avg}}} \tag{17}$$

where *k(0)* is the fluctuating coefficient for in-phase six-step method which is defined as

$$k(0) = \frac{3}{4\pi}\int_0^{\theta_\alpha}\left(\frac{2}{3}\cos\theta - \frac{2}{\pi}\right)\mathrm{d}\theta \cong 0.00145. \tag{18}$$

Equation (17) shows that the amplitude of the fluctuating dc-link voltage in flying capacitor is proportional to the input power and inversely proportional to the capacitance, the average dc-link voltage, and the rotational speed. Thus, it is obvious that the fluctuation problem becomes negligible in the high speed region.

C. Six-Step Operation in Low Speed Region

In the low speed region, back-EMF of the machine is not high and the required active voltage is also low. Therefore, it is impossible to use in-phase six-step method for *Inv*1. In [35], SVPWM method is utilized to adjust the active power transferred to the system. Because the output torque is limited by not voltage but current, modulation method does not affect the output torque.

The SVPWM method in the low speed region of dual inverter with flying capacitor system, however, suffers from several problems: huge dc current harmonics, high switching loss, and transition shock between modulation methods. As aforementioned, six-step modulation method reduces huge dc-link

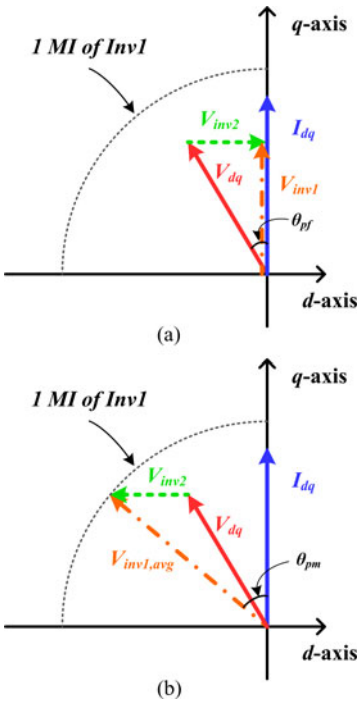

Fig. 12. Vector diagrams of dual inverter system at low speed region. (a) In-phase modulation. (b) Phase shift modulation.

current harmonics from PWM and helps the filter reduction. PWM operation in low speed region, however, impedes the reduction of the filter and harms the battery. Although the high-speed operation does not require the heavy filter, it is hard to reduce the filter due to the severe harmonic current in the low-speed region. The switching loss is also can be reduced with the six-step operation. The transition shock between SVPWM and six-step modulation also causes a problem in dual inverter with flying capacitor system. SVPWM used in low speed region can output the voltage up to 0.9069 MI. Because the six-step methods supplies fixed 1 MI voltage, the transition around the rated speed region causes torque ripple and instability issue in control system. For these reasons, another modulation method for low speed region is demanded for dual inverter with flying capacitor system.

This paper proposes a phase modulation to solve these problems. The phase modulation methods was widely researched for high speed dc–dc conversion circuit such as dual active bridge [39], [40], and phase shift converter [41]. Similar to these methods, it is possible to adjust the power in the dual inverter system using phase modulation method. Fig. 12 shows the vector diagrams of the average voltage and current in synchronous reference frame. In the conventional method, output voltages of the two inverters are decided orthogonally to decouple the power as shown in the Fig. 12(a). In this case, however, amplitude of the V_{inv1} becomes lower than the unity MI and should be chopped by switching. For the six-step phase modulation method, amplitude of the V_{inv1} is fixed to unity MI as represented in Fig. 12(b). The instantaneous output voltage of the six-step phase modulation method is defined similarly with Table II. By replacing the

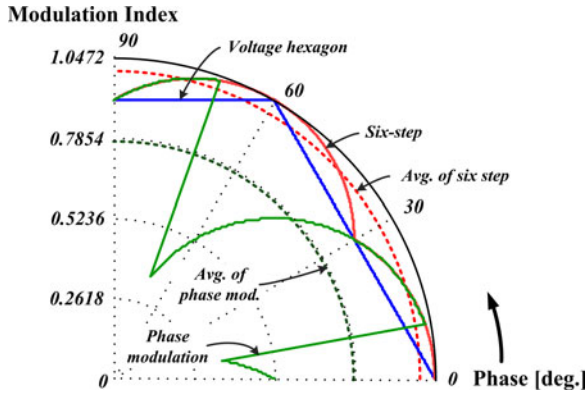

Fig. 13. Instantaneous active output voltage of the six step phase modulation method in stationary reference frame from 0° to 90° when $\theta_{\rm pm}$ is 40°.

current angle to the average voltage angle, from θ_i to $\theta_i + \theta_{\rm pm}$, where $\theta_{\rm pm}$ is the phase modulation angle defined as the phase difference between current and modulated V_{inv1}. For example, when the $\theta_{\rm pm}$ is 40° and θ_i is 5°, V_{inv1} is decided to vertex no. 2. If the $\theta_{\rm pm}$ is 40° and θ_i is $-20°$, V_{inv1} is located on vertex no. 1. Phase modulated voltage $V_{inv1,\rm avg}$ is decided to transfer same amount of active power to the system. Thus, the average active component of the V_{inv2} becomes zero.

The active component voltage from the *Inv1* can be mathematized as

$$V_{inv1,\rm act} = \frac{2}{\pi} V_{\rm dc1} \cos\theta_{\rm pm} \tag{19}$$

where $\theta_{\rm pm}$ is the most important value for the phase modulation method and can be obtained with current reference and active voltage as

$$\theta_{\rm pm} = \cos^{-1}\left(V_{\rm act} \Big/ \frac{2}{\pi} V_{\rm dc1}\right). \tag{20}$$

Because two solutions for (20) always exist, the selection procedure for the optimal solution is required. Both solutions give the same active voltage but the amplitudes of reactive voltages generated by six-step are different each other. By selecting the optimal $\theta_{\rm pm}$, it is possible to moderate the compensation burden of the *Inv*2. Because $V_{\rm dc2}$ can be controlled with the lower value with this properly selected $\theta_{\rm pm}$, the inverter loss can be reduced. The optimal value of $\theta_{\rm pm}$ can be acquired by comparing it with θ_{pf}. Choosing $\theta_{\rm pm}$ which has same sign with θ_{pf} gives optimal $\theta_{\rm pm}$ that can minimizes the reactive voltage for the *Inv*2.

Fig. 13 shows the phase modulated six-step voltage in the stationary reference frame when the $\theta_{\rm pm}$ is 40°. Because the voltage is shifted, the active voltage applied to the load is not maximized and the average is also diminished. Fig. 14 shows $V_{inv1,\rm act}$ of the proposed six-step phase modulation method in Cartesian coordinate when $\theta_{\rm pm}$ are 5° and 40°. Comparing to the Fig. 11, it is easy to find out that the step changing points move $\theta_{\rm pm}$ from $-30°$ to $-25°$ and 10°, respectively. The average modulation voltages are also reduced to 0.996 and 0.766 proportionally to the cosine of the $\theta_{\rm pm}$.

The only demerit of the phase modulation method is the increased fluctuation in power and $V_{\rm dc2}$. Because the six-step

TABLE III
FLUCTUATION COEFFICIENT OF SIX-STEP PHASE MODULATION

Section	θ_{pm}	Fluctuation coefficient (k)
I	$-180° \le \theta_{pm} < -180°+ \theta_{crit}$ $-\theta_{crit} \le \theta_{pm} < \theta_{crit}$ $180°- \theta_{crit} \le \theta_{pm} < 180°$	$\frac{3}{4\pi}\int_0^{\theta_\alpha}\left(\frac{2}{3}\cos\theta - \frac{2}{\pi}\cos\theta_{pm}\right)d\theta$
II	$-180°+ \theta_{crit} \le \theta_{pm} < -\theta_{crit}$ $\theta_{crit} \le \theta_{pm} < 180° - \theta_{crit}$	$\frac{3}{8\pi}\int_{\theta_{pm}-30°}^{\theta_\alpha}\left(\frac{2}{3}\cos\theta - \frac{2}{\pi}\cos\theta_{pm}\right)d\theta$

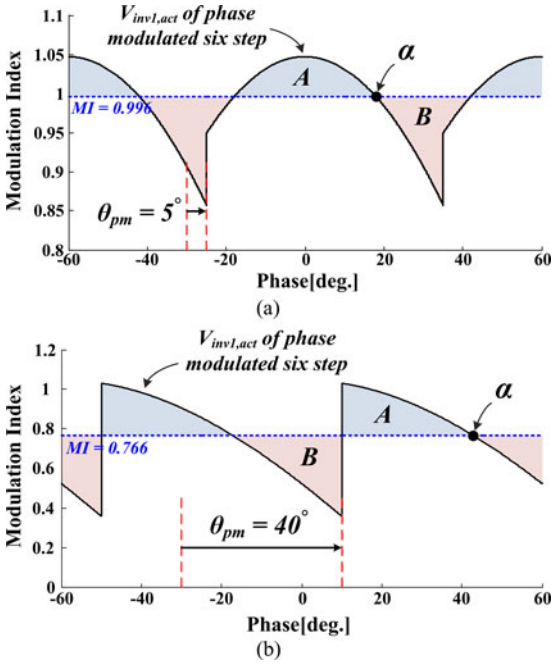

Fig. 14. Active voltage of phase modulated six-step method in Cartesian coordinate. (a) When $\theta_{\rm pm}$ is 5°. (b) When $\theta_{\rm pm}$ is 40°.

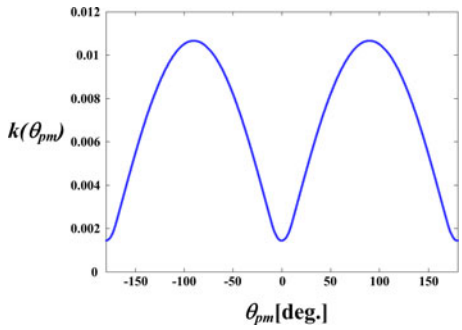

Fig. 15. Fluctuation coefficient $k(\theta_{\rm pm})$ according to the $\theta_{\rm pm}$.

phase modulation method generates higher fluctuating power, ΔV is higher than that of the in-phase six-step method in the high speed region. This is because not only the frequency is low but also the fluctuating active voltage is high. The fluctuating voltage varies according to $\theta_{\rm pm}$ and is calculated in two different regions. When $\theta_{\rm pm}$ is low, the area A still remains symmetric as shown in Fig. 14(a). Although the area B is not symmetric, it is easily calculated from A, because the extents of A and B are same. This symmetry is maintained until the step change angle of the instant active voltage exceeds the average active voltage output. This relation about the critical angle can be depicted as (21) and (22)

$$\frac{2}{3}V_{\rm dc1}\cos(\theta_{\rm crit} - 30°) = \frac{2}{\pi}V_{\rm dc1}\cos\theta_{\rm pm} \tag{21}$$

$$\theta_{\rm crit} = \tan^{-1}\left(\frac{6}{\pi} - \sqrt{3}\right) = 10.08°. \tag{22}$$

Using the symmetry about $\theta_{\rm pm}$, it is possible to divide the calculation region as listed in Table III. For the first section, the area can be integrated using the symmetry as

$$S_A = 2\int_0^{\theta_\alpha}\left(\frac{2}{3}V_{\rm dc1}\cos\theta - \frac{2}{\pi}V_{\rm dc1}\cos\theta_{\rm pm}\right)d\theta. \tag{23}$$

When $\theta_{\rm pm}$ is higher than $\theta_{\rm crit}$, the area A also becomes asymmetric as shown in Fig. 14(b). Thus, integration of area A for the second section can be depicted as

$$S_A = \int_{\theta_{\rm pm}-30°}^{\theta_\alpha}\left(\frac{2}{3}V_{\rm dc1}\cos\theta - \frac{2}{\pi}V_{\rm dc1}\cos\theta_{\rm pm}\right)d\theta. \tag{24}$$

For (23) and (24), θ_α is the point where instantaneous active output voltage becomes same with average output and can be calculated as

$$\theta_\alpha = \cos^{-1}\left(\frac{3}{\pi}\cos\theta_{\rm pm}\right). \tag{25}$$

With the equations depicted previously, the fluctuation coefficient $k(\theta_{\rm pm})$ can be drawn as in Fig. 15. The power fluctuation is maximized when the current vector and V_{inv1} are orthogonal. Because the fluctuation coefficient at 90° is approximately eight times higher than the in-phase case, dc-link voltage fluctuation becomes considerable in this situation. Furthermore, because the phase modulation method is applied in low speed region, voltage ripple in flying dc link becomes considerable and have to be taken into account in design stage.

D. Field Weakening Control

High speed operation is the main purpose of the dual inverter with flying capacitor system and it cannot be operated without the field weakening control. Many field weakening control methods have been suggested for several decades [1]–[8]. Among

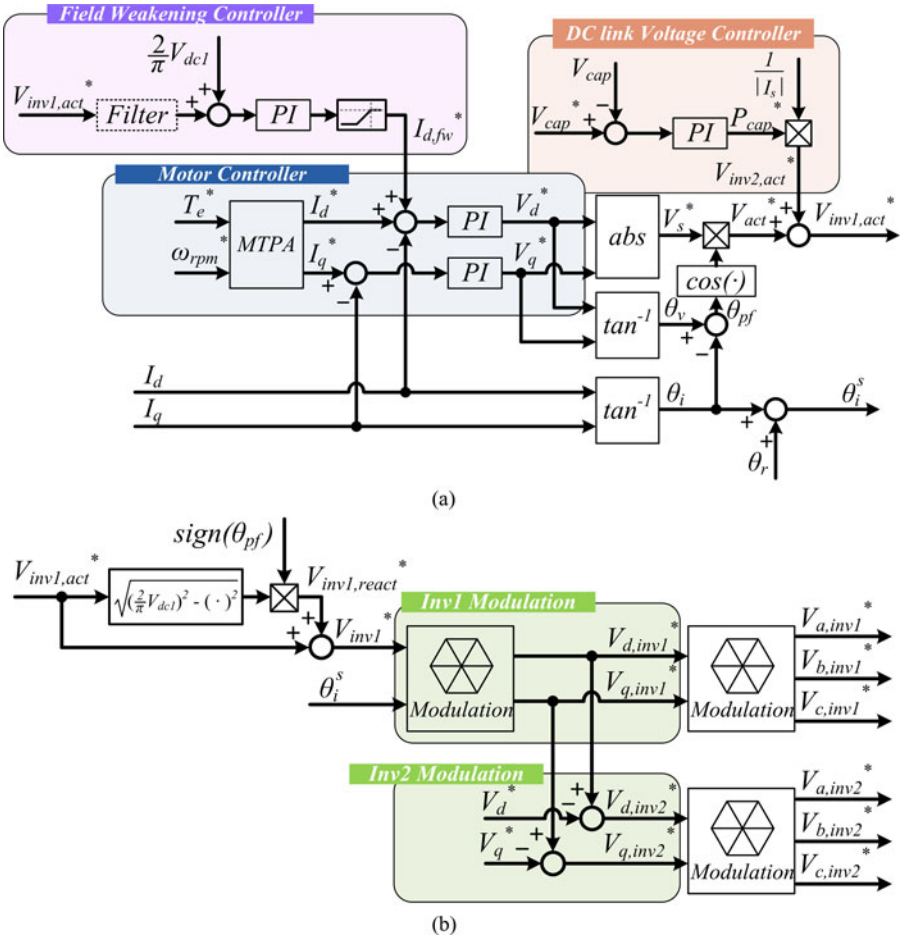

Fig. 16. Configuration of controller for six-step modulation of dual inverter with flying inverter. (a) Motor, field weakening, and dc-link voltage controller. (b) Phase modulator and voltage modulation stage.

them, this paper introduces the voltage feedback method only because it is free from the load parameters and simple to apply [8]. This method just feeds the output voltage reference back and regulates it by lowering *d*-axis current. The biggest difference between the field weakening control of single inverter system and that of dual inverter with flying capacitor system is the voltage which is fed back. The field weakening control generally used for the single inverter system regulates the output reference voltage to the linear range. For the dynamic performance and the control stability, the voltage limit is set to have 5%–10% margin. Thus, the voltage limit becomes (26) when SVPWM is applied

$$V_{\lim} = \eta \frac{V_{\mathrm{dc}}}{\sqrt{3}} \tag{26}$$

where η is voltage margin coefficient which generally has value around 0.9–0.95. In the previous studies, this limited voltage is applied to the dual inverter system and limits output voltage. This marginal voltage can be considered as a wasted voltage. For the dual inverter system with six step modulation, the voltage limit goes up to 1 MI regardless of margin and the voltage limit can be written as (27)

$$V_{\lim} = \frac{2}{\pi} V_{\mathrm{dc1}}. \tag{27}$$

Thus, the voltage wasted for the margin can be eliminated. This output voltage maximization minimizes field weakening current and improves system efficiency. Furthermore, the increment is not the apparent power but the pure active power. Therefore, this increment effect is not negligible.

The active voltage reference for the *Inv*1 includes the active voltage for the load and V_{dc2} regulation. Whereas the active voltage for the load becomes constant in steady state, the active voltage required for regulating V_{dc2} fluctuates due to the six-step operation. For this reason, the *d*-axis current also becomes fluctuating. The fluctuating current generates errors in controller. Thus, this fluctuating component should be minimized for stable operation. It can be reduced by lowering the cut-off frequency of the field weakening controller. This method, however, also lowers the dynamic performance of the system such as acceleration, deceleration, and V_{dc2} regulation. Because fluctuating voltage of V_{dc2} is mainly composed of six times of rotating frequency, it also can be filtered by low pass or notch filter. This method can lessen the current fluctuation while it maintains the dynamic performance.

TABLE IV
PARAMETERS OF THE MACHINE AND EXPERIMENTAL CONDITIONS

Category	Value
Number of the poles(n_p)	8
Phase resistance(R_s)	0.013 [Ω]
Phase inductance(L_s)	1.8 [mH]
Flying capacitance(C_{dc2})	3.3[mF]
Back-EMF constant(λ_f)	0.129 [V·s]
Power source dc link voltage(V_{dc1})	60 [V]
Flying dc link voltage(V_{dc2})	150 [V]
Rated current	25 [A]

Below the rated speed region, the *d*-axis current for field weakening should be controlled to zero for MTPA operation. Thus, the field weakening controller only works when θ_{pm} is zero. The composition of field weakening controller is in the following section.

E. System Control

The controller of the proposed six-step modulation for dual inverter with flying capacitor is composed as shown in Fig. 16. Fig. 16(a) shows the motor controller, field weakening controller, and flying dc-link voltage controller, and Fig. 16(b) shows the voltage modulation stage. Motor controller part is quite similar with the conventional motor controller. It is composed of MTPA table or algorithm and two PI current regulators which control *d–q* axis currents in the synchronous reference frame. Output active voltage required to the motor is calculated with the outputs of the two current regulators, V_d^* and V_q^*. DC-link voltage controller is also necessary to control the flying dc-link voltage. It is simply composed of one PI regulator. It gives the power required to the flying dc link and it is converted to the active voltage reference ${V_{inv2,\mathrm{act}}}^*$. Two active voltage references are added and become the active voltage reference of the *Inv*1. Phase modulation algorithm is applied after calculating ${V_{inv1,\mathrm{act}}}^*$ and gives the reactive voltage reference ${V_{inv1,\mathrm{react}}}^*$. The output voltage references are modulated with six-step for *Inv*1. The current angle and rotor position are required to convert voltages and currents between *d–q* components and active/reactive components. The field weakening controller also gives *d*-axis current reference. Field weakening current controller regulates ${V_{inv1,\mathrm{act}}}^*$ to 1 MI. This controller can contain low pass filter or notch filter for the better performance.

IV. EXPERIMENTAL RESULTS

To verify the validity of the proposed control method, experiments are accomplished with a PMSM. The parameters of the machine and experimental conditions are listed in the Table IV. DC-link voltage of the power source is 60 V and the flying dc-link voltage is controlled to 150 V. Instead of the battery, dc power supply is simply adopted as a power source. Although the flying dc-link voltage can be controlled according to the operating condition, it is fixed to 150 V to compare the efficiency. For *Inv*1, the power MOSFET IRFP4468s with nominal $R_{\mathrm{ds,on}}$ of 2.0 mΩ were used. For *Inv*2, the intelligent power module PM150RLA060 of 600 V rating voltage and 150 A rating current was used.

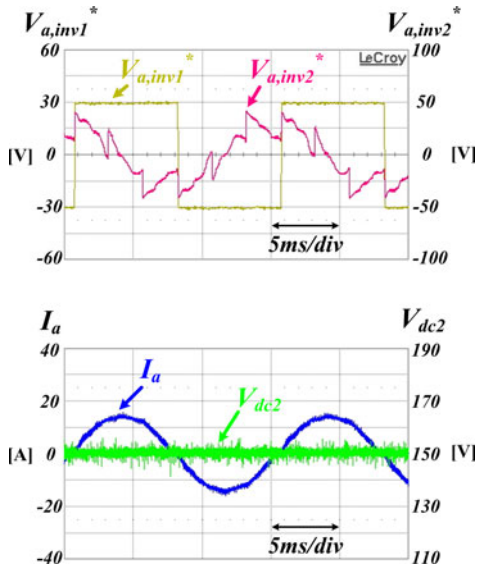

Fig. 17. Key waveforms of the proposed hybrid modulation for dual inverter with flying inverter at 1000 r/min.

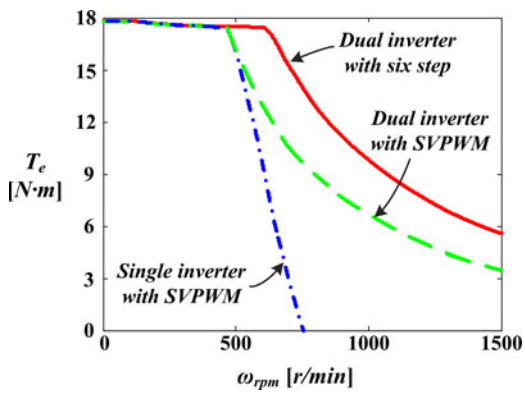

Fig. 18. Operation area of the PMSM according to the driving methods.

Fig. 17 shows the key waveforms of the in-phase six-step modulation method for dual inverter with flying capacitor when the machine rotates at 1000 r/min. Four waveforms in Fig. 17 are the A phase voltage references for the each inverter, A phase current, and flying capacitor voltage. It definitely shows that current waveforms are pure sinusoidal even though *Inv*1 operates with six-step. It remarks that the torque ripples are not caused by the six-step operation of *Inv*1. The current ripples also can be minimized by adjusting V_{dc2} in accordance with the operating condition.

Fig. 18 shows the experimentally achieved operation areas of the machine according to the three different driving methods. As verified in the previous researches of [31] and [32], operation area of the dual inverter with flying capacitor is much larger than that of the single inverter case. Similar to the analyzed results depicted in Fig. 10(a), adopting the six-step operation to *Inv*1 increases the output power and enlarges operation area.

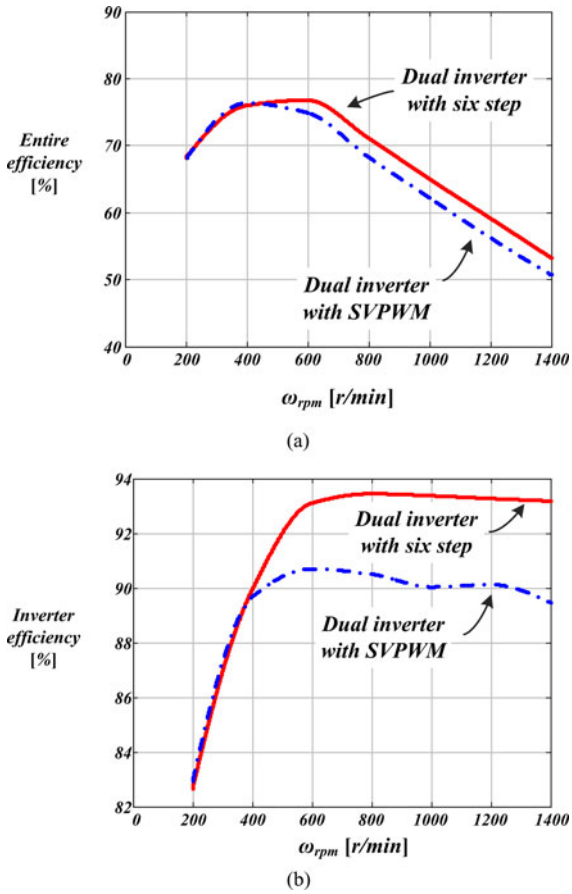

Fig. 19. Efficiency comparison for the two modulation methods. (a) Entire efficiency. (b) Inverter efficiency.

Fig. 19 shows the entire efficiency including motor loss and the inverter efficiency, respectively. The entire driving efficiency is achieved with the calculated output power based on machine parameter and input power measured with PM6000 manufactured by Voltech. Inverter efficiency is also measured with the PM6000. Because the maximum output torques of the two operation methods are different, the efficiency comparison result for the maximum load case is meaningless. Thus, the half of the maximum torque of the proposed method is equally loaded to the both operation methods. As shown in the Fig. 19, entire efficiency and inverter efficiency of the proposed method are much higher than those of the conventional method. Because the inverter and motor are not operated in the rated condition, the efficiency is not high for the both cases. However, the experimental results clearly verify the efficiency enhancing effect of the proposed method.

Fig. 20 shows the key waveforms of the phase modulation method for dual inverter with flying capacitor topology. Each waveform indicates the A phase voltage references for *Inv*1 and *Inv*2, current, and V_{dc2} at 200 r/min. As shown in Fig. 20, phase current is still regulated as a sinusoidal waveform regardless of the modulation method. The active power required to the machine is controlled by the phase difference of V_{inv1} and current, and the waveforms of V_{a,inv_1} and I_a verify the power

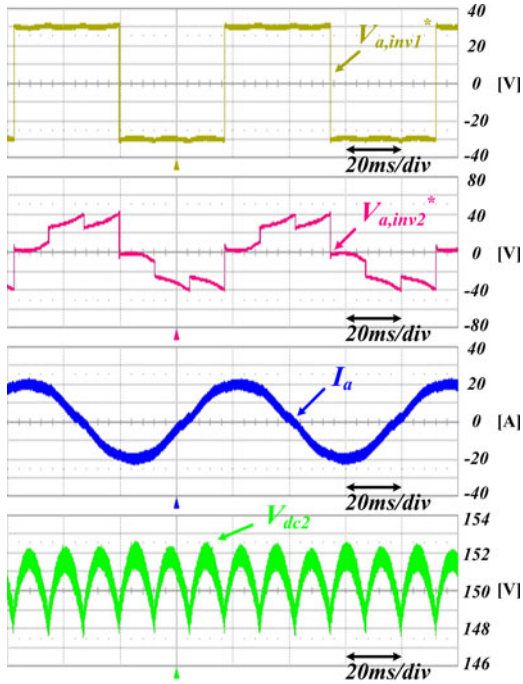

Fig. 20. Experimental waveforms of the proposed hybrid modulation method at 200 r/min.

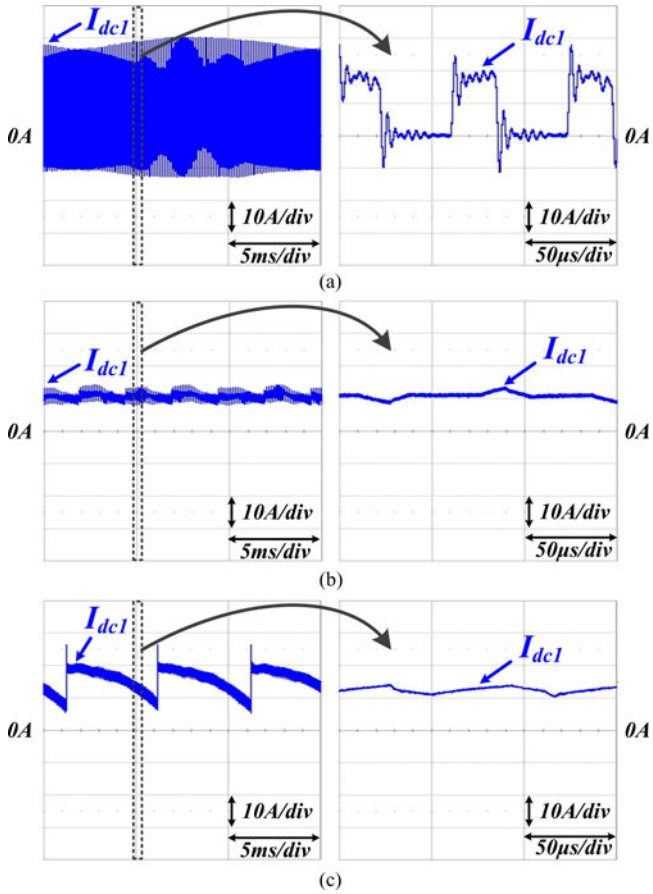

Fig. 21. DC-link current waveforms of the three different modulation methods. (a) SVWPM. (b) In-phase six-step method. (c) Phase modulated six-step method.

regulation capability of the proposed method. Waveform of $V_{\mathrm{dc}2}$ shows the fluctuating voltage according to the six-step operation. It definitely shows that the ripple frequency of $V_{\mathrm{dc}2}$ is six times of the fundamental one. This fluctuation becomes severer in low speed operation and should be considered in system design stage.

Fig. 21 shows the dc-link currents of *Inv*1 according to the modulation methods. Experiments for the SVPWM operation is executed at 200 r/min, in-phase six-step operation are executed at 1000 r/min, and the experiment for the phase modulation operation is executed at 500 r/min. As shown in Fig. 21(a), the dc-link current waveform of SVPWM adopted case is chopped by the switching of *Inv*1. This dc-link current can deteriorate the battery health and life, and cause the severe EMI. As shown in Fig. 21(b), dc-link current is smoothed by the continuous conduction of *Inv*1, and only contains the ripple from the *Inv*2 switching filtered by the inductance of the machine. It is obvious that the smoothed dc-link current can reduce the input filter and EMI. For the phase shift method case as in Fig. 21(c), the dc-link current is still continuous but changes abruptly in every 60°. This discontinuous current chopping comes from the nonzero current switching of *Inv*1. It can obstruct the filter minimizing, but it is much lighter than the conventional filter.

V. Conclusion

This paper presents the hybrid modulation method which uses hybrid modulation which combines the six-step modulation and SVPWM for dual inverter with flying capacitor topology. The proposed modulation method features the high efficiency and wide operation area. It maximizes the advantages of the dual inverter system and minimizes the defects such as battery current ripple and high inverter loss. The proposed method enlarges the six-step operation area to the whole operation region including the low speed where the conventional method cannot operate. Thanks to the six-step operation of the battery side inverter in whole operation region, the battery side dc-link filter can be reduced. This paper analyzes the modulation method especially considering the power flow between the inverter and motor. The field weakening method and controller for the proposed method are also presented. The reduced scale experiments with the PMSM are also executed to verify the superiority of the proposed method. The experimental results prove that the proposed method gives the high efficiency and large operation area.

References

[1] J.-K. Seok and S.-K. Sul, "Optimal flux selection of an induction machine for maximum torque operation in flux-weakening region," *IEEE Trans. Power Electron.*, vol. 14, no. 4, pp. 700–708, Jul. 1999.

[2] M. Tursini, E. Chiricozzi, and R. Petrella, "Feedforward flux-weakening control of aurface-mounted permanent-magnet synchronous motors accounting for resistive voltage drop," *IEEE Trans. Ind. Electron.*, vol. 57, no. 1, pp. 440–448, Jan. 2010.

[3] T.-S. Kwon and S.-K. Sul, "Novel antiwindup of a current regulator of a surface-mounted permanent-magnet motor for flux-weakening control," *IEEE Trans. Ind. Appl.*, vol. 42, no. 5, pp. 1293–1300, Sep./Oct. 2006.

[4] S. Kim and J.-K. Seok, "Maximum voltage utilization of IPMSMs using modulating voltage scalability for automotive applications," *IEEE Trans. Power Electron.*, vol. 28, no. 12, pp. 5639–5646, Dec. 2013.

[5] A. Tripathi, A. M. Khambadkone, and S. K. Panda, "Dynamic control of torque in overmodulation and in the field weakening region," *IEEE Trans. Power Electron.*, vol. 21, no. 4, pp. 1091–1098, Jul. 2006.

[6] M. Mengoni, L. Zarri, A. Tani, G. Serra, and D. Casadei, "A comparison of four robust control schemes for field-weakening operation of induction motors," *IEEE Trans. Power Electron.*, vol. 27, no. 1, pp. 307–320, Jan. 2012.

[7] H. Liu, Z. Q. Zhu, E. Mahamed, Y. Fu, and X. Qi, "Flux-weakening control of nonsalient pole PMSM having large winding inductance, accounting for resistive voltage drop and inverter nonlinearities," *IEEE Trans. Power Electron.*, vol. 27, no. 2, pp. 942–952, Feb. 2012.

[8] J.-M. Kim and S.-K. Sul, "Speed control of interior permanent magnet synchronous motor drive for the flux weakening operation," *IEEE Trans. Ind. Appl.*, vol. 33, no. 1, pp. 43–48, Jan./Feb. 1997.

[9] C.-H. Kim, M.-Y. Kim, H.-S. Park, and G.-W. Moon, "A modularized two-stage charge equalizer with cell selection switches for series-connected lithium-ion battery string in an HEV," *IEEE Trans. Power Electron.*, vol. 27, no. 8, pp. 3764–3774, Aug. 2012.

[10] M. Einhorn, W. Roessler, and J. Fleig, "Improved performance of serially connected Li-ion batteries with active cell balancing in electric vehicles," *IEEE Trans. Veh. Technol.*, vol. 60, no. 6, pp. 2448–2457, Jul. 2011.

[11] A. M. Imtiaz and F. H. Khan, ""Time shared flyback converter" based regenerative cell balancing technique for series connected Li-ion battery strings," *IEEE Trans. Power Electron.*, vol. 28, no. 12, pp. 5960–5975, Dec. 2013.

[12] S. J. Moura, J. L. Stein, and H. K. Fathy, "Battery-health conscious power management in plug-in hybrid electric vehicles via electrochemical modeling and stochastic control," *IEEE Trans. Contr. Syst. Technol.*, vol. 21, no. 3, pp. 679–694, May 2013.

[13] Z. Zheng, K. Wang, L. Xu, and Y. Li, "A hybrid cascaded multilevel converter for battery energy management applied in electric vehicles," *IEEE Trans. Power Electron.*, vol. 29, no. 7, pp. 3537–3546, Jul. 2014.

[14] J. O. Estima and A. J. Marques Cardoso, "Efficiency analysis of drive train topologies applied to electric/hybrid vehicles," *IEEE Trans. Veh. Technol.*, vol. 61, no. 3, pp. 1021–1031, Mar. 2012.

[15] Z. Du, B. Ozpineci, L. M. Tolbert, and J. N. Chiasson, "DC–AC cascaded H-bridge multilevel boost inverter with no inductors for electric/hybrid electric vehicle applications," *IEEE Trans. Ind. Appl.*, vol. 45, no. 3, pp. 963–970, May/Jun. 2009.

[16] F. Z. Peng, "Z-source inverter," *IEEE Trans. Ind. Appl.*, vol. 39, no. 2, pp. 504–510, Mar./Apr. 2003.

[17] M. Shen, A. Joseph, J. Wang, F. Z. Peng, and D. J. Adams, "Comparison of traditional inverters and Z-source inverter for fuel cell vehicles," *IEEE Trans. Power Electron.*, vol. 22, no. 4, pp. 1453–1463, Jul. 2007.

[18] F. Guo, L. Fu, C.-H. Lin, C. Li, W. Choi, and J. Wang, "Development of an 85-kw bidirectional quasi-Z-source inverter with DC-link feed-forward compensation for electric vehicle applications," *IEEE Trans. Power Electron.*, vol. 28, no. 12, pp. 5477–5488, Dec. 2013.

[19] O. Ellabban, J. V. Mierlo, and P. Lataire, "A DSP-based dual-loop peak DC-link voltage control strategy of the Z-source inverter," *IEEE Trans. Power Electron.* vol. 27, no. 9, pp. 4088–4097, Sep. 2012.

[20] K. R. Sekhar and S. Srinivas, "Discontinuous decoupled PWMs for reduced current ripple in a dual two-level inverter fed open-end winding induction motor drive," *IEEE Trans. Power Electron.*, vol. 28, no. 5, pp. 2493–2502, May 2013.

[21] V. T. Somasekhar, S. Srinivas, and K. K. Kumar, "Effect of zero-vector placement in a dual-inverter fed open-end winding induction-motor drive with a decoupled space-vector PWM strategy," *IEEE Trans. Ind. Electron.*, vol. 55, no. 6, pp. 2497–2505, Jun. 2008.

[22] S. Srinivas and K. R. Sekhar, "Theoretical and experimental analysis for current in a dual-inverter-fed open-end winding induction motor drive with reduced switching PWM," *IEEE Trans. Ind. Electron.*, vol. 60, no. 10, pp. 4318–4328, Oct. 2013.

[23] V. T. Somasekhar, K. Gopakumar, M. R. Baiju, K. K. Mohapatra, and L. Umanand, "A multilevel inverter system for an induction motor with open-end windings," *IEEE Trans. Ind. Electron.*, vol. 52, no. 3, pp. 824–836, Jun. 2005.

[24] V. T. Somasekhar, S. Srinivas, and K. K. Kumar, "Effect of zero-vector placement in a dual-inverter fed open-end winding induction motor drive with alternate sub-hexagonal center PWM switching scheme," *IEEE Trans. Power Electron.*, vol. 23, no. 3, pp. 1584–1591, May 2008.

[25] C. Patel, R. P. P. A. Day, A. Dey, R. Ramchand, K. Gopakumar, and M. P. Kazmierkowski, "Fast direct torque control of and open-end induction motor drive using 12-sided polygonal voltage space vectors," *IEEE Trans. Power Electron.*, vol. 27, no. 1, pp. 400–410, Jan. 2012.

[26] Y. Wang, D. Panda, T. A. Lipo, and D. Pan, "Open-winding power conversion systems fed by half-controlled converters," *IEEE Trans. Power Electron.*, vol. 28, no. 5, pp. 2427–2436, May 2013.
[27] M.-S. Kwak and S.-K. Sul, "Control of an open-winding machine in a grid-connected distributed generation system," *IEEE Trans. Ind. Appl.*, vol. 44, no. 4, pp. 1259–1267, Jul./Aug. 2008.
[28] S. D. G. Jayasinghe, D. M. Vilathgamuwa, and U. K. Madawala, "Direct integration of battery energy storage systems in distributed power generation," *IEEE Trans. Energy Convers.*, vol. 26, no. 2, pp. 677–685, Jun. 2011.
[29] S. D. G. Jayasinghe, D. M. Vilathgamuwa, and U. K. Madawala, "A dual inverter-based supercapacitor direct integration scheme for wind energy conversion systems," *IEEE Trans. Ind. Appl.*, vol. 49, no. 3, pp. 1023–1030, May/Jun. 2013.
[30] J. Hong, H. Lee, and K. Nam, "Charging method for the second battery in dual-inverter drive systems for electric vehicles," in *Proc. IEEE 29th Annu. Appl. Power Electron. Conf. Expo.*, Mar. 16–20, 2014, pp. 2407–2414.
[31] J. Kim, J. Jung, and K. Nam, "Dual-Inverter control strategy for high-speed operation of EV induction motors," *IEEE Trans. Ind. Electron.*, vol. 51, no. 2, pp. 312–320, Apr. 2004.
[32] D. Pan, F. Liang, Y. Wang, and T. A. Lipo, "Extension of the operating region of an IPM motor utilizing series compensation," *IEEE Trans. Ind. Appl.*, vol. 50, no. 1, pp. 539–548, Jan./Feb. 2014.
[33] J. Ewanchuk, J. Salmon, and C. Chapelsky, "A method for supply voltage boosting in an open-ended induction machine using a dual inverter system with a floating capacitor bridge," *IEEE Trans. Power Electron.*, vol. 28, no. 3, pp. 1348–1357, Mar. 2013.
[34] T. Gerrits, C. G. E. Wijnands, J. J. H. Paulides, and J. L. Duarte, "Dual voltage source inverter topology extending machine operating range," in *Proc. IEEE Energy Convers. Conf. Exhibit.*, Sep. 2012, pp. 2840–2846.
[35] Y. Lee and J.-I. Ha, "Power enhancement of dual inverter for open-end permanent magnet synchronous motor," in *Proc. IEEE Appl. Power Electron. Conf. Expo.*, Mar. 2013, pp. 1545–1551.
[36] P. Rao, M. L. Crow, and Z. Yang, "STATCOM control for power system voltage control applications," *IEEE Trans. Power Del.*, vol. 15, no. 4, pp. 1311–1317, Oct. 2000.
[37] P. D. Evans and R. J. Hill-Cottingham, "DC link current in PWM inverters," *IEE Proc. B*, vol. 133, no. 4, pp. 217–224, Jul. 1986.
[38] M. Uno and K. Tanaka, "Influence of high-frequency charge-discharge cycling induced by cell voltage equalizers on the life performance of lithium-ion cells," *IEEE Trans. Veh. Technol.*, vol. 60, no. 4, pp. 1505–1515, May. 2011.
[39] B. Zhao, Q. Song, and W. Liu, "Power characterization of isolated bidirectional dual-active-bridge DC–DC converter with dual-phase-shift control," *IEEE Trans. Power Electron.*, vol. 27, no. 9, pp. 4172–4176, Sep. 2012.
[40] H. Bai and C. Mi, "Eliminate reactive power and increase system efficiency of isolated bidirectional dual-active-bridge DC–DC converters using novel dual-phase-shift control," *IEEE Trans. Power Electron.*, vol. 23, no. 6, pp. 2905–2914, Nov. 2008.
[41] I.-H. Cho, K.-M Cho, J.-W Kim, and G.-W. Moon, "A new phase-shifted full-bridge converter with maximum duty operation for server power system," *IEEE Trans. Power Electron.*, vol. 26, no. 12, pp. 3491–3500, Dec. 2011.

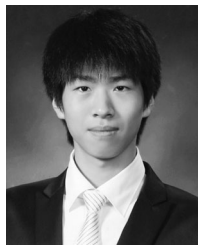

Yongjae Lee (S'12) received the B.S. and M.S. degrees in electrical engineering from Seoul National University, Seoul, Korea, in 2011 and 2013, respectively, where he is currently working toward the Ph.D. degree.

His current research interests include electric machine drives and power electronics.

Jung-Ik Ha (S'97–M'01–SM'12) was born in Korea, in 1971. He received the B.S., M.S., and Ph.D. degrees in electrical engineering from Seoul National University, Seoul, Korea, in 1995, 1997, and 2001, respectively.

From 2001 to 2002, he was a Researcher in Yaskawa Electric Co., Japan. From 2003 to 2008, he worked for Samsung Electronics Co., Korea as a Senior and Principal Engineer. From 2009 to 2010, he was a Chief Technology Officer, LS Mechapion Co., Korea. Since 2010, he has been an Assistant Professor of the School of Electrical Engineering, Seoul National University, Seoul. His research interests include circuits and control in high efficiency and integrated electric energy conversions for various industrial fields.